# Hybrid Propagation Physics for The Design and Modeling of Astronomical Observatories Outfitted with Coronagraphs

**Jaren N. Ashcraft**[a], **Ewan S. Douglas**[b], **Daewook Kim**[a,b,c], **A.J. Riggs**[d]
[a]James C. Wyant College of Optical Sciences, University of Arizona, Meinel Building 1630 E. University Blvd., Tucson, AZ. 85721
[b]Department of Astronomy and Steward Observatory, University of Arizona, 933 N. Cherry Ave., Tucson, AZ 85719, USA
[c]Large Binocular Telescope Observatory, University Of Arizona, 933 N. Cherry Ave. Tucson, AZ 85721
[d]Jet Propulsion Laboratory, California Institute of Technology, 4800 Oak Grove Drive, Pasadena, CA 91109

**Abstract.** For diffraction-limited optical systems an accurate physical optics model is necessary to properly evaluate instrument performance. Astronomical observatories outfitted with coronagraphs require physical optics models to simulate the effects of misalignment,[?] diffraction,[?] and polarization.[?] Accurate knowledge of the observatory's point-spread function (PSF) is integral for the design of high-contrast imaging instruments[?] and simulation of astrophysical observations.[?] The state of the art models the misalignment, ray aberration, and diffraction model across multiple software packages, which complicates the design process.[?] This research proposes to update an existing, powerful open-source optical analysis software (POPPY) with new propagation physics to better integrate the geometrical and physical regimes of the optical field. Gaussian Beamlet Decomposition is a ray-based method of diffraction calculation that has been widely implemented in commercial optical design software.[?,?] By performing the coherent calculation with data from the ray model of the observatory the ray aberration errors can be fed directly into the physical optics model of the coronagraph, enabling a more integrated and open-source model of the observatory.

**Keywords:** physical optics modeling, coronagraphs, Fresnel, Gaussian Beamlet Decomposition.

*Jaren N. Ashcraft, jashcraft@email.arizona.edu

## 1 Introduction

### *1.1 Astrophysical Motivation*

High-contrast imaging instruments have been deployed on the ground (e.g. SCExAO,[1] MagAO-X[2]) and in space (e.g. NICMOS,[?] NIRCam[?]) to pursue the direct detection of extrasolar planets and exozodiacal dust. The Astro2020 Decadal Survey has identified that pursuing these instruments for the next generation of observatories is a key priority for the progression of astrophysical sciences.[?] Currently there exists a gap between the theoretical limit on coronagraph performance and what modern realizations of these instruments are actually able to achieve. This is in part due to the sensitivity of coronagraphs to low-order aberrations minimizing the raw contrast achievable

near the inner working angle (IWA).[3] We hypothesize that this performance gap can be spanned by providing a better connection between the ray trace model of the observatory and the wave propagation model of the coronagraph.

Integrated models of optical observatories are highly beneficial to their use and design.[?] Open-source packages in particular have been widely used to simulate the performance of high-contrast imaging instrumentation. Tiny Tim was one of the first of these widely-used packages used to simulate the Hubble Space Telescope (HST) instrument point-spread functions (PSF).[4] The tool generates aberrated PSFs based on the instrument, observation, and dynamic aberrations for a given observing scenario, enabling highly accurate simulations of the observatory performance. However, this tool only considered aberrations that were conjugate to the exit pupil of the observatory. This limits the model's ability to capture out-of-pupil effects, like the Talbot effect and speckle from optical surfaces. To provide integrated modeling capabilities to future observatories, tools like PROPER,[5] POPPY,[6] and HCIPy[7] were developed. These PSF simulation packages further integrated optical models of observatories by adding Fresnel diffraction to the PSF simulation, enabling the modeling of plane-to-plane diffraction effects. Near-field diffraction effects that limited high-contrast imaging could be modeled, and novel focal-plane wavefront sensing methods could be tested. FALCO[8] is a similar tool that uses the same propagation physics to aid the design of these instruments by optimizing the commands sent to a deformable mirror to correct for the near-field diffraction effects that could limit the Roman Coronagraph's Sensitivity. These open-source physical optics propagation tools form the cornerstone of high-contrast imaging instrument modeling and design, but they do not exist in a vacuum. To account for effects that aren't traceable through the assumptions made by Fresnel diffraction, these models must be linked to other software. Presently the optical design of observatories are done in a ray-tracing engine (e.g. CODE

V, OpticStudio) because it is more suitable to optimizing the shapes of observatory mirrors. Upon reaching a diffraction-limited optical design, the system is then assumed to be well-represented by a paraxial diffraction model. The wavefront maps produced by the ray trace model of the observatory and the contributions from the imperfect polishing of the observatory mirrors are sent to an open-source physical optics code (e.g. PROPER, POPPY, HCIPy) to examine the image plane field in the presence of diffraction from structure in the beam and phase errors on the optics.

| Design Code | Ray Trace | Wave Propagation | Open Source |
|---|---|---|---|
| CODE V | ✓ | ✓ | |
| OpticStudio | ✓ | ✓ | |
| FRED | ✓ | ✓ | |
| POPPY | | ✓ | ✓ |
| HCIPy | | ✓ | ✓ |
| PROPER | | ✓ | ✓ |

**Table 1** Comparison of commonly-used software's ability to ray trace, do physical optics, and be open source. Consider replacing with a table.

While this approach has been suitable to the modeling of an instrument's PSF, it is less integrated, and makes the assumption that the optical field is well-represented by Fresnel diffraction. Commercial optical design codes offer the ability to make diffraction calculations based on ray data, but their physical optics simulation techniques aren't as transparent or versatile as the open-source propagation codes that are used to design coronagraphs for astronomical observatories. The current open-source physical optics codes used for observatory modeling are also limited in their scope because of the Fresnel approximation, which is incapable of accurately modeling the field after fast-focusing surfaces, highly aspheric[9] surfaces, and non-uniform pupils.[10] As observatories get larger, their optics must become faster and more aspheric to fit within a reasonable volume. Some coronagraph architectures capable of earthlike exoplanet detection (e.g. PIAA[?]) employ mirrors that apodize the pupil with highly aspheric mirrors, and require tailored propagators in

order to be included in physical optics models.[9] In the regime where the contribution of these surfaces is best represented by a ray trace, a diffraction calculation must be made to appropriately model the optical field at the image plane.

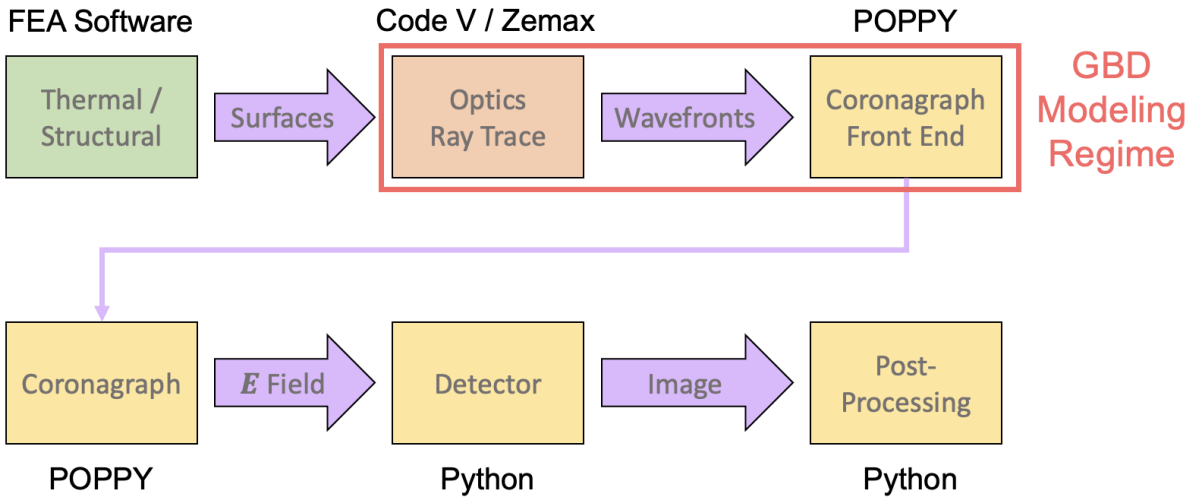


**Fig 1** Modeling flow inspired by the STOP modeling process for Roman Coronagraph.[?] This diagram illustrates the different software packages and their associated modeling regimes. The dashed red box shows the region that could be unified using Gaussian Beamlet Decomposition as a propagation technique, which would open-source the ray-based physical optics of ray tracing codes.

To bridge the gap between commercial ray tracing engines and open-source physical optics propagation codes we investigate the viability of a ray-based diffraction calculation for designing observatories with coronagraphs called Gaussian Beamlet Decomposition (GBD). The technique has been previously implemented in commercial codes (CODE V,[?] FRED[?]) and been recently developed to improve its viability for precision diffraction simulation.[11–13] However, the method has not seen wide implementation in the world of open-source physical optics propagators, and has not yet been formally evaluated as a tool to augment the modeling of observatories equipped with high-contrast imaging instrumentation.

### *1.2 Gaussian Beamlet Decomposition*

Gaussian Beamlet Decomposition (GBD) is a method of physical optics propagation that approximates the propagated field as a finite sum of Gaussian beams. This method has been implemented in many optical design packages[14] to perform coherent calculations on non-paraxial systems. Fourier transform-based propagation methods derived from the Huygens-Fresnel diffraction integral typically assume the field is scalar and optical system is paraxial.[15] This is a fair assumption for astronomical coronagraphs which operate on slowly focusing beams with diffraction-limited optics. Astronomical observatories however, employ fast mirrors with conic surfaces to collect a large amount of light in a relatively short instrumental volume. Observatories are designed and modeled in ray trace software to accurately model the wavefront in the exit pupil. Upon finalizing the design, the complex exit pupil is sent to a Fourier-based physical optics propagator to simulate the performance of a high-contrast imaging instrument. GBD aims to compute the same complex optical field without making the paraxial assumption across the instrument. Rather, the propagation of a generally astigmatic Gaussian beam is derived from the Collins integral[?,16] which imposes the paraxial assumption about a single Gaussian beamlet, which is a much less stringent approximation. Gaussian's are technically infinite in extent, but 99% of the energy is enclosed within the $2/e$ irradiance radius. Consequently, the contribution of the field very far from the Gaussian is negligible. This parameter enables the optical system to generally be non-paraxial, providing that the beamlets are not very divergent.[17]

### *1.3 Hybrid Propagation Physics*

The ray-based nature of GBD introduces problems in modeling the electric field when the rays are vignetted. For a Lyot-type coronagraph all rays are vignetted at the focal plane mask which

eliminates the field decomposition. To circumvent this we compute the field before the focal plane mask with GBD and propagate it through the remaining coronagraph with Fresnel diffraction. This *hybrid* method enables the user to alter the propagation physics for the electric field based on where it is the most appropriate.

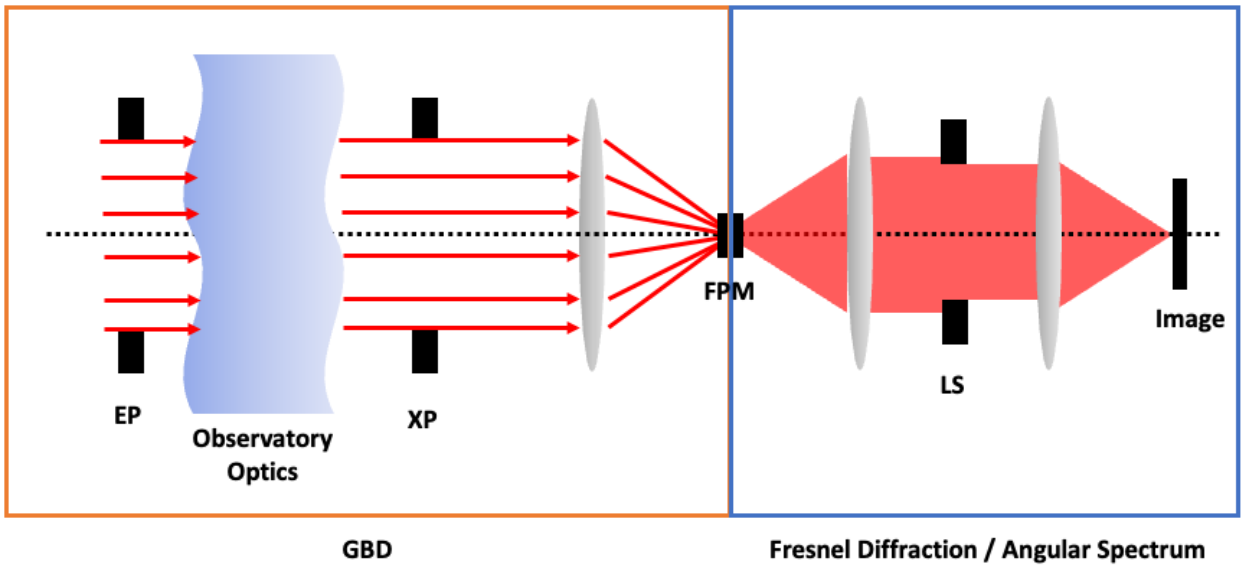


**Fig 2** Diagram demonstrating the hybrid propagation physics model. The observatory optics are best described by a ray-based propagation model, so GBD is used to compute the field at the image plane before the coronagraph FPM. The field array is then handed to a Fresnel propagation model which propagates it past the FPM and through the remainder of the coronagraph.

The end result of such a model allows for direct integration of the ray trace model with the physical optics model, without imposing the paraxial approximation on the observatory. Like Fresnel, GBD is an approximation to diffraction physics. The decomposition of the field into gaussian beams does not have a unique solution. Therefore, undesirable artifacts can be introduced into the field if the decomposition is not well-understood and the sampling is insufficient.[18] To better understand the impact of a GBD PSF on high-contrast imaging simulations, we develop a hybrid propagation model to compare GBD to an equivalent Fresnel diffraction model. In section 2 we outline the mathematics of the Gaussian Beam and how it is used to simulate an observatory

PSF. In section 3 we compare the results of observatory PSFs produced by GBD with one produced using traditional Fourier transform-based diffraction methods. In section 4 we assess the suitability of GBD for high-contrast imaging models and establish a roadmap for our module's development.

## 2 Methods

To assess the viability of GBD for high-contrast imaging simulation we first compare the point-spread function (PSF) produced by GBD to one produced by an equivalent Fresnel diffraction model for a given observatory. This comparison is done to assess the ability of GBD to achieve Fresnel-equivalent performance using the same assumptions. The Fresnel model is built with the open-source package POPPY (Physical Optics Propagation in PYthon), which was developed to simulate the PSFs of the James Webb Space Telescope.[19] Fresnel diffraction represents the state of the art for coronagraph modeling because of the method's capacity to model near-field effects that limit high-contrast imaging (e.g. the Talbot effect[15]). Our GBD module's capacity to model Fresnel-equivalent phenomena[18] has been illustrated in a previous investigation, so we now investigate its feasibility to produce an accurate model of an observatory's PSF. In this section we illustrate the operating principles of Gaussian beam propagation and how they are used to simulate arbitrary fields.

### *2.1 Gaussian Beam Parameters*

To propagate an arbitrary optical beam the field must be decomposed into a finite sum of Gaussian beamlets which are then independently propagated. A single Gaussian Beam is described entirely

by the complex beam parameter $q(z)$:[15]

$$U(r,z) = \frac{U_o}{q(z)} exp[ik\frac{r^2}{2q(z)}] \tag{1}$$

Where $U_o$ is the amplitude, $k$ is the wavenumber, and $r$ is the radial coordinate in the plane perpendicular to propagation. The complex parameter $q(z)$ describes the beam's $1/e$ field size (the "waist" $w_o$) and wavefront radius of curvature $R(z)$.

$$q(z)^{-1} = \frac{1}{R(z)} + i\frac{\lambda}{\pi w(z)^2} \tag{2}$$

$q(z)$ is a convenient expression of the Gaussian beam because it fully encapsulates the information required to describe the transverse electric field of the beam as it propagates. The real part of $q(z)$ is related to the radius of curvature of the wavefront.

$$R(z) = z(1 + (\frac{Z_o}{z})^2) \tag{3}$$

Where $Z_o$ is the Rayleigh range and $z$ is the longitudinal propagation distance. The imaginary part of $q(z)$ is related to the beam waist radius

$$w(z) = w_o\sqrt{1 + (\frac{z}{Z_o})^2} \tag{4}$$

In the paraxial regime $q(z)$ can be propagated using the ABCD ray transfer matrices of geometrical optics.

$$q(z)_o^{-1} = \frac{C + D/q_i}{A + B/q_i} \tag{5}$$

For the generally astigmatic case, $q(z)$ is a 2x2 matrix $\mathbf{Q}(z)$ that encodes the complex curvature in two orthogonal directions and how they couple into each other.[16,18]

$$\mathbf{Q}(z)^{-1} = \begin{pmatrix} q(z)_{xx}^{-1} & q(z)_{xy}^{-1} \\ q(z)_{yx}^{-1} & q(z)_{yy}^{-1} \end{pmatrix} \tag{6}$$

This treatment allows for greater versatility in the beamlet propagation, but requires that the elements of the ray transfer matrices are also 2x2 matrices. The propagation of the generally decentered and astigmatic Gaussian beam is described in Cai and Lin,[16] which derives an expression of the beam propagation purely in terms of matrix optics. By leveraging this unique parameter of the Gaussian beam we can perform diffraction calculations without traditional Fourier-transform based methods. The full equation in matrix form is given in equation 7.

$$U(\vec{r}_o) = \frac{e^{ikl_o}}{|\mathbf{A} + \mathbf{B}\mathbf{Q_1^{-1}}|^{1/2}} e^{-\frac{ik}{2}\vec{r_o}^T \mathbf{Q_2}^{-1} \vec{r_o}} e^{-\frac{ik}{2}\vec{r_i}^T (\mathbf{Q_1}^{-1} + \mathbf{A}^{-1}\mathbf{B})\vec{r_i}} e^{ik\vec{r_i}^T (\mathbf{A}\mathbf{Q_1}^{-1} + \mathbf{B})\vec{r_o}} \tag{7}$$

Note that the arguments of the exponential are scalar valued quantities, and are represented in matrix form for brevity.

### *2.2 Entrance Pupil Spatial Decomposition*

The operating principle of GBD is to decompose the field in the optical system's entrance pupil into a finite sum of Gaussian beamlets. Our module spatially decomposes the field at the entrance pupil and propagates each beamlet along a ray path using equation 7. Various sample schemes exist in the literature, with different strengths and weaknesses. The "even" sample scheme described in Harvey et al[17] is the most straightforward, where the beamlets lie evenly spaced along a square

grid. The ray coordinates in the entrance pupil are then computed from an overlap factor (OF) which describes the overlap of the beamlets $1/e$ waist radii $w_o$.[12]

$$OF = \frac{N_g 2\omega_o}{W} \tag{8}$$

Where $N_g$ is the number of Gaussian beamlets across an aperture, and $W$ is the width of the aperture. This feature is easy to implement and understand, but for under-sampled cases it introduces artifacts due to the ripple and soft edge left by the Gaussian beamlets. The "Fibonacci" sample scheme introduced by Worku and Gross[12] places the beamlets along a Fibonacci spiral such that the RMS error of the decomposed field is minimized. Hexapolar sampling is also a viable method to increase the accuracy of the decomposition for fewer beamlets assuming the optical system has a circular aperture.[12] Both sample schemes are not well-matched to Cartesian grids, so applying wavefront error arrays to optical elements requires interpolation of the surface, which slows the simulation. For the results presented in this paper, we employ the even sample scheme.

### *2.3 Paraxial Model w/ Arbitrary WFE*

First we construct a paraxial model of the observatory to compare GBD against Fresnel diffraction for modeling astronomical observatories and their coronagraphs. The paraxial model carries the same assumptions of Fresnel diffraction: that the angles are small and that all optics are gaussian reduced to their principal planes.[15] This comparison will show that GBD is suitable to mimicing the performance of Fresnel diffraction-based propagators. In the paraxial assumption ray propagation is handled by ray transfer matrices for propagation (**D**) and refraction (**L**)[18]

$$\mathbf{L} = \begin{pmatrix} 1 & 0 & 0 & 0 \\ 0 & 1 & 0 & 0 \\ -1/f_x & 0 & 1 & 0 \\ 0 & -1/f_y & 0 & 1 \end{pmatrix}; \mathbf{D} = \begin{pmatrix} 1 & 0 & d/n & 0 \\ 0 & 1 & 0 & d/n \\ 0 & 0 & 1 & 0 \\ 0 & 0 & 0 & 1 \end{pmatrix} \tag{9}$$

Where $\mathbf{L}$ is the matrix representing a thin lens of focal length $f$ and $\mathbf{D}$ is the matrix representing the propagation of rays by a distance $d$. The generally nonorthogonal optical system permits propagation through optics with focal lengths that are not equal in $x$ and $y$, but for the paraxial model all lenses are set such that $f_x = f_y$. Constructing an optical system with these matrices is done by taking their matrix product.

$$\mathbf{O_{sys}} = \prod_{i=1}^{N} \mathbf{D}_i \mathbf{L}_i \tag{10}$$

Where a general optical system can be reduced to $N$ interactions of a refraction by the $i$-th optic $\mathbf{L}_i$ and propagation by the $i$-th distance $\mathbf{D}_i$.

Low-order aberrations are of importance to the design of coronagraphs for observatories because they spread the PSF over the focal plane mask which couples starlight into the high-contrast region of the coronagraph. Consequently tracing the low-order aberrations accurately is of paramount importance to any propagation physics used for high-contrast imaging modeling. In the paraxial regime, we model wavefront errors on optics with Jeong et al's arbitrary wavefront error ray transfer matrix.[20] For a given optical path difference $W(x, y)$ the nonorthogonal ray transfer matrix can be computed by calculating the gradient of the wavefront error function.

$$\mathbf{W}(x,y) = \begin{pmatrix} 1 & 0 & 0 & 0 \\ 0 & 1 & 0 & 0 \\ \frac{1}{x}\frac{\partial W(x,y)}{\partial x} & 0 & 1 & 0 \\ 0 & \frac{1}{y}\frac{\partial W(x,y)}{\partial y} & 0 & 1 \end{pmatrix} \tag{11}$$

Where $x, y$ are the coordinates of the ray incident on the surface with wavefront error $W$. Jeong et al showed the analytical computations of wavefront error as a sum of Zernike polynomials, but in this investigation we used numpy's gradient function to compute the wavefront error for any arbitrary array. Doing this decreases the number of matrix products needed to describe the optical system. However, each ray path must encounter a different ray transfer matrix for derivatives of $W$ that are not constant. The effective paraxial optical system is given by $\mathbf{O}_{paraxial}$

$$\mathbf{O}_{paraxial} = \mathbf{DLW} \tag{12}$$

Such that the wavefront is aberrated, focused, and then propagated to the image plane. This investigation will simply evaluate GBD in the case where it is trying to employ the same assumptions as Fresnel diffraction with entirely different physics, without the benefits of modeling non-paraxial effects.

### *2.4 Nonparaxial Model with Differential Ray Tracing*

The key benefit of using GBD for observatory modeling is its ability to model the PSF of an observatory using ray data. The paraxial assumption is only made along a single raypath, so coherent calculations can be done for generally nonparaxial systems. However, to use Cai and Lin's equation to propagate the beamlet the ray transfer matrix must be solved for every ray in the

optical system. To do so we implement differential ray tracing to solve the matrix in terms of the derivatives of the ray data. Differential ray tracing is a key tool in optical design software used in a variety of applications.[?,21] We employ this technique by using a ray tracing engine (Zemax OpticStudio) that propagates rays by computing Snell's Law at each surface. A local coordinate system is defined for both the input and output surface, and the ray derivatives are computed using the finite differences method. An example of computing the element $A_{x,x}$ is given by equation 13. In this example two rays are traced, one with a differential addition in input $x$ coordinate and one with no change. The $x$ coordinates of these input and output rays determine the derivative.

$$A_{xx} = \frac{\partial x_2}{\partial x_1} = \frac{x_{output,+x} - x_{output,o}}{x_{input,+x} - x_{input,o}} \tag{13}$$

The ray transfer matrix for a non-orthogonal optical system has 16 unknowns, and each ray yields 4 quantities. To solve for every element of the matrix 4 linearly independent rays must be traced. The simplest ray set is geometrically orthogonal,[22] where copies of the central ray $(x, y, u, v)$ are modified by a differential quantity $(\delta)$ in each of the 4 ray coordinates.

$$\begin{pmatrix} x+\delta x \\ y \\ u \\ v \end{pmatrix}, \begin{pmatrix} x \\ y+\delta y \\ u \\ v \end{pmatrix}, \begin{pmatrix} x \\ y \\ u+\delta u \\ v \end{pmatrix}, \begin{pmatrix} x \\ y \\ u \\ v+\delta v \end{pmatrix} \tag{14}$$

The ray of interest is propagated along with four rays that enable the computation of the local derivatives in position $(x, y)$ and angle $(u, v)$. The full differential ray transfer matrix is given by

equation 15. The ray transfer matrix is purely a function of the Cartesian position of the ray $(x, y)$ and slope of the ray in those directions $(u, v)$ at the input and output of the optical system.

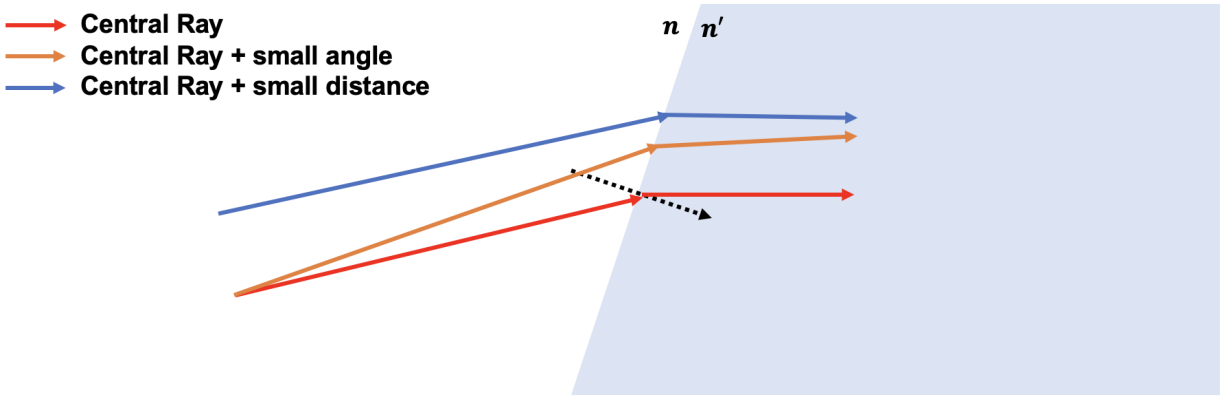


**Fig 3** Diagram illustrating differential ray tracing in the 2D case on a locally planar interface between media with incident refractive index $n$ and transmitted refractive index $n'$. The black dotted line indicates the surface normal for the interaction with the central ray.

$$\begin{pmatrix} x' & y' & u' & v' \end{pmatrix} = \begin{pmatrix} \frac{\partial x_2}{\partial x_1} & \frac{\partial x_2}{\partial y_1} & \frac{\partial x_2}{\partial u_1} & \frac{\partial x_2}{\partial v_1} \\ \frac{\partial y_2}{\partial x_1} & \frac{\partial y_2}{\partial y_1} & \frac{\partial y_2}{\partial u_1} & \frac{\partial y_2}{\partial v_1} \\ \frac{\partial u_2}{\partial x_1} & \frac{\partial u_2}{\partial y_1} & \frac{\partial u_2}{\partial u_1} & \frac{\partial u_2}{\partial v_1} \\ \frac{\partial v_2}{\partial x_1} & \frac{\partial v_2}{\partial y_1} & \frac{\partial v_2}{\partial u_1} & \frac{\partial v_2}{\partial v_1} \end{pmatrix} \begin{pmatrix} x \\ y \\ u \\ v \end{pmatrix} \tag{15}$$

Because Gaussian beamlets are propagated along geometric ray paths, computing the differential ray transfer matrix enables the propagation of a beamlet through an arbitrary optical system. Using this matrix any open-source diffraction model can be linked to a ray trace model of an observatory.

### *2.5 Accelerated Computing*

The independence of the Gaussian beamlet operations are uniquely suited to the exploration of multi-threaded computation to accelerate diffraction simulations. Accelerated computing is inte-

gral to diffraction modeling to enable rapid and precision simulation of small signals. The time to conduct traditional Fourier-based diffraction modeling is set by the complexity of the system. The sampling of each optical element and the number of total optical elements increase the complexity and number of Fast Fourier Transforms (FFT) used, resulting in more computation time. GBD circumvents the FFT entirely by tracing rays to propagate through the optical system in a fraction of the time of the FFT. GBD's diffraction calculation at the plane of interest computes an exponential of an array that scales with the number of beamlets and sampling of the image plane, resulting in longer computation times. Preliminary explorations into accelerated computing were conducted using the numexpr[?] and numba[23] Python packages that showed favorable computation time decreases by multi-threading the operation on a CPU. Both packages operate by pre-compiling a given function into machine code that the program calls and breaking up the operation into chunks of arrays that a CPU core can handle efficiently. The key computational advantage of GBD is the ability to do diffraction calculations in parallel. Numba was the first package explored due to its ease of implementation. The package works by applying a decorator to a Python function that processes the large array of interest, and then specifying the number of central processing unit (CPU) cores for the process to use. The distribution of the information stored within the array is handled automatically by numba, and results in considerable runtime decreases for GBD. On a 16 core 2.4GHz CPU, runtime for a simulation of 1876 Gaussian beamlets through a coronagraph to simulate a 256x256 pixel focal plane was sped up by a factor of 5, which approached POPPY's Fresnel diffraction runtime. This experiment was repeated using the numexpr package which showed an even greater decrease in computation time. The comparison in runtime vs. number of CPU cores is shown in Fig. 6.

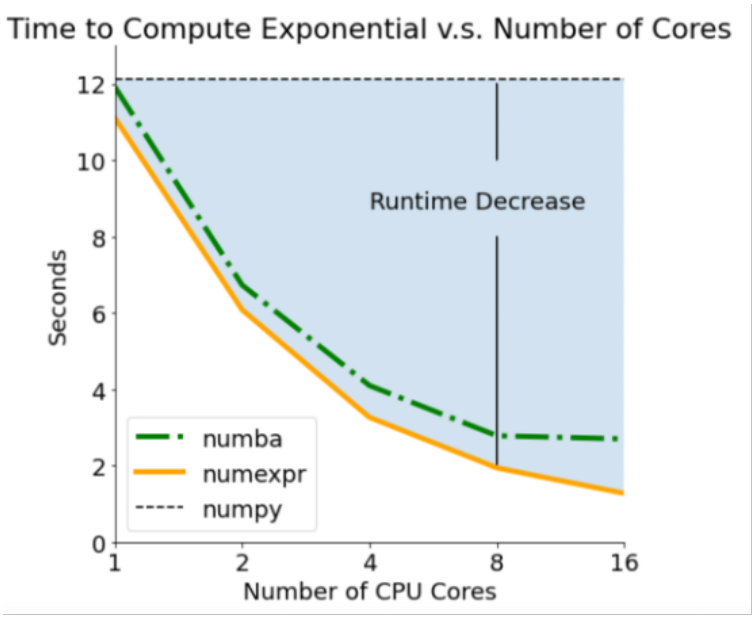


**Fig 4** Run time comparison for a 50x50 grid of Gaussian beamlets on a 256 x 256 detector grid v.s. number of CPU cores used.

We anticipate even greater speedups on graphical processing units (GPU), and intend to add GPU compatibility to our GBD module in future work.

## 3 Results

To evaluate GBD as a viable physical optics propagation technique we must evaluate its performance v.s. Fresnel diffraction for a given observatory. The fiducial observatory used in this study is a Ritchey-Chretien (RC) objective based on the Hubble Space Telescope (HST). This model is developed both in Zemax OpticStudio and as a paraxial optical system to compare the propagation methods. The system prescription is given in table 2 and the effective ray transfer matrix is given in equation 16.

| Surface | RoC [m] | Conic Constant | Distance [m] | Semi-Aperture [m] |
|---|---|---|---|---|
| M1 | -11.0400 | -1.00230 | -4.90607 | 1.20000 |
| M2 | -1.35800 | -1.49686 | 6.40620 | 0.14056 |

**Table 2** Optical system prescription for the RC telescope based on the HST used in this investigation. All distances are given in meters.

$$\mathbf{O_{RC}} = \begin{pmatrix} 0 & 0 & 57.6 & 0 \\ 0 & 0 & 0 & 57.6 \\ -0.0174 & 0 & 1 & 0 \\ 0 & -0.0174 & 0 & 1 \end{pmatrix} \tag{16}$$

The equivalent paraxial optical system (Fresnel, paraxial GBD) can't be easily modeled because the mirrors aren't well-represented by the quadratic phase surface characteristic of thin lenses in diffraction modeling software. Rather, the observatory will be modeled as though it was a single thin lens inside the entrance pupil of the telescope with focal length equal to the total focal length of the telescope. Aberrations are applied to the non-paraxial model by perturbing the position of the secondary mirror. The same aberrations are applied to the paraxial models by doing a Zernike polynomial decomposition on the wavefront phase in the exit pupil. These phase aberrations are applied in the pupil of the paraxial model and propagated to focus.

### *3.1 The Fiducial Coronagraph*

The fiducial coronagraph for this study is a charge-2 vector vortex coronagraph (VVC). The complex amplitude of the focal plane mask is

$$U(x, y) = exp[i2arctan(\frac{y}{x})] \tag{17}$$

and the transmission is unity everywhere except for the center pixel, where it is 0. This is because there is a singularity in the phase ramp at this location, so it must be masked out. We chose the VVC because of its ability to effectively reject on-axis starlight at a given wavelength. Should GBD introduce undesirable artifacts into the PSF, it should be visible in the coronagraphic

focal plane. The VVC used in this simulation necessitated very high sampling (16k x 16k array) in order to resolve the singularity.

### *3.2 Paraxial Model*

The Fresnel-equivalent models of the observatory PSFs and the coronagraphic PSFs for our HST model with a circular aperture are shown below in figures 5 and 6, respectively. The observatory PSF comparison in figure 5 has the analytical airy function for an equivalent telescope aperture subtracted to reveal the computational residuals from using this diffraction method.

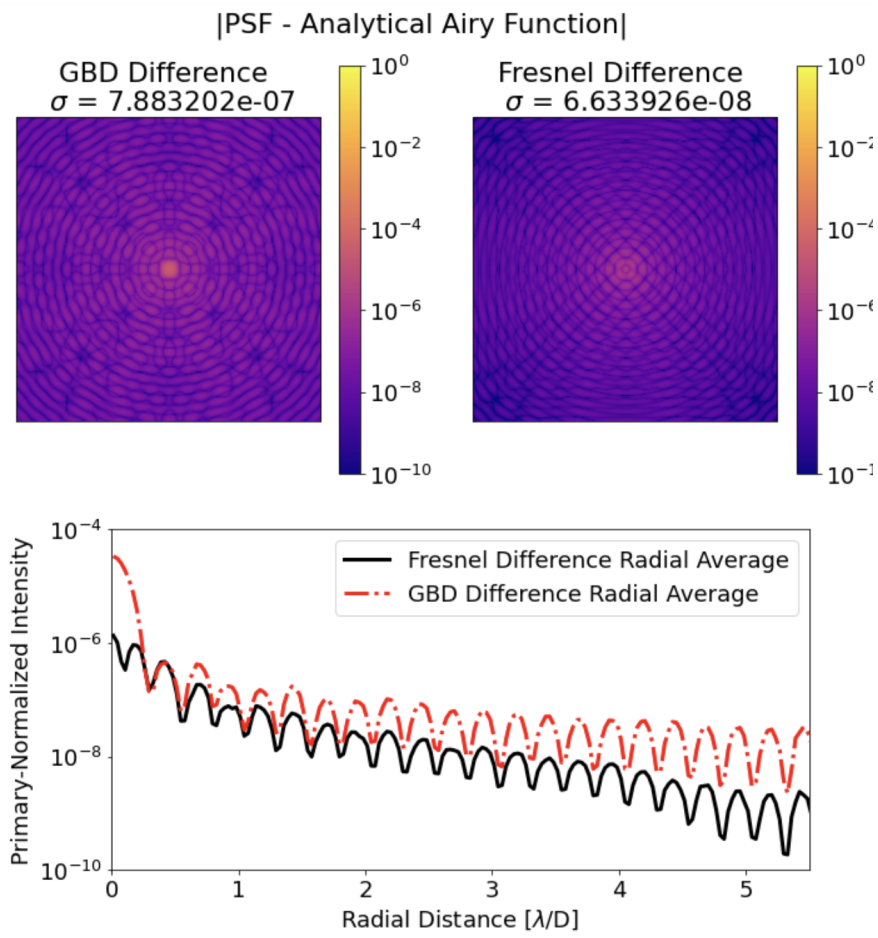


**Fig 5** Comparison of the PSF generated by paraxial GBD (left) and Fresnel (middle) for the same optical system with the analytical result subtracted. The azimuthally averaged radial profile is plotted to clarify the discrepancy in the PSF (bottom).

Neither reproduce the airy function exactly, which is an expectation of any finite simulation. The discrepancy in the GBD PSF comes from the characteristic ripple from the beamlet distribution, and the inability to fully reconstruct a sharp-edge aperture. The discrepancy in the Fresnel PSF comes from the discretization of the circular pupil. Both simulations can be improved by higher sampling, but this comes as substantially greater computational cost. To understand the influence of these residual errors they must be propagated through the fiducial coronagraph model. We also inject a faint and incoherent off-axis source for this simulation to illustrate a case of imaging a planetary companion.

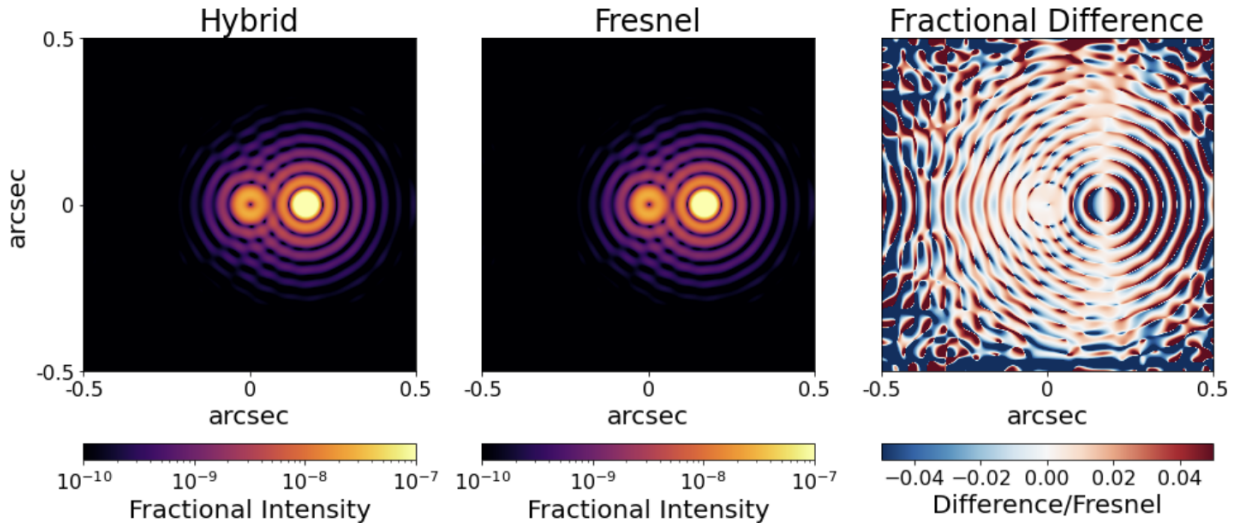


**Fig 6** Comparison of the Coronagraphic PSF without aberration generated by paraxial GBD (left) and Fresnel (middle) and the fractional difference of the PSFs (right). The RMS difference of the PSFs is on the order of $3 \times 10^{-11}$.

The coronagraphic images show an encouraging congruence. By inspection the images shown in Figure 6 are nearly identical. The fractional difference shows that where there is actually power in the image the difference is negligible, indicating the suitability of the proposed hybrid propagation scheme for creating fresnel-equivalent models of observatories outfitted with coronagraphs.

### *3.3 Real Model*

While the paraxial results are an encouraging first demonstration of GBD's ability to accurately simulate an observatory PSF, the real power of the technique lies in its ability to connect a Fresnel model of a coronagraph to a ray trace model of an observatory. Shown below are the PSF simulations using the differential ray tracing methods detailed in Section 2.

**Fig 7** Comparison of the PSF generated by non-paraxial GBD (left) and Fresnel (middle) for the same optical system and the difference of the PSFs (right). The azimuthally averaged radial profile is plotted to clarify the discrepancy in the PSF (bottom).

**Fig 8** Comparison of the Coronagraphic PSF generated by non-paraxial GBD (left) and Fresnel (middle) for the same optical system and the difference of the PSFs (right). The azimuthally averaged radial profile is plotted to clarify the discrepancy in the PSF (bottom).

## 4 Conclusion

*References*


1 J. Lozi, O. Guyon, N. Jovanovic, *et al.*, "SCExAO, an instrument with a dual purpose: perform cutting-edge science and develop new technologies," *Adaptive Optics Systems VI* , 270 (2018). arXiv: 1809.08301.

2 J. R. Males, L. M. Close, K. L. Miller, *et al.*, "MagAO-X: project status and first laboratory results," in *Adaptive Optics Systems VI*, D. Schmidt, L. Schreiber, and L. M. Close, Eds., 9, SPIE, (Austin, United States) (2018).

3 S. e. a. Shaklan, "Status of space-based segmented-aperture coronagraphs for characterizing exo-earths around sun-like stars," (2019).

4 J. Krist, "Tiny Tim : an HST PSF Simulator," in *Astronomical Data Analysis Software and Systems II*, R. J. Hanisch, R. J. V. Brissenden, and J. Barnes, Eds., *Astronomical Society of the Pacific Conference Series* **52**, 536 (1993).

5 J. E. Krist, "PROPER: an optical propagation library for IDL," in *Optical Modeling and Performance Predictions III*, M. A. Kahan, Ed., **6675**, 250 – 258, International Society for Optics and Photonics, SPIE (2007).

6 E. S. Douglas and M. D. Perrin, "Accelerated modeling of near and far-field diffraction for coronagraphic optical systems," in *Space Telescopes and Instrumentation 2018: Optical, Infrared, and Millimeter Wave*, M. Lystrup, H. A. MacEwen, G. G. Fazio, *et al.*, Eds., **10698**, 864 – 877, International Society for Optics and Photonics, SPIE (2018).

7 E. H. Por, S. Y. Haffert, V. M. Radhakrishnan, *et al.*, "High Contrast Imaging for Python (HCIPy): an open-source adaptive optics and coronagraph simulator," in *Adaptive Optics Systems VI*, *Proc. SPIE* **10703** (2018).

8 A. E. Riggs, G. Ruane, C. T. Coker, *et al.*, "Fast linearized coronagraph optimizer (FALCO) IV: coronagraph design survey for obstructed and segmented apertures," in *Space Telescopes and Instrumentation 2018: Optical, Infrared, and Millimeter Wave*, H. A. MacEwen, M. Lystrup, G. G. Fazio, *et al.*, Eds., 167, SPIE, (Austin, United States) (2018).

9 J. E. Krist, L. Pueyo, and S. B. Shaklan, "Practical numerical propagation of arbitrary wavefronts through PIAA optics," 77314N, (San Diego, California, USA) (2010).

10 R. J. Vanderbei, "Diffraction Analysis of Two-dimensional Pupil Mapping for High-Contrast Imaging," *The Astrophysical Journal* **636**, 528–543 (2006).

11 N. G. Worku and H. Gross, "Vectorial field propagation through high NA objectives using polarized Gaussian beam decomposition," in *Optical Trapping and Optical Micromanipulation XIV*, K. Dholakia and G. C. Spalding, Eds., 33, SPIE, (San Diego, United States) (2017).

12 N. G. Worku, R. Hambach, and H. Gross, "Decomposition of a field with smooth wavefront

into a set of gaussian beams with non-zero curvatures," *J. Opt. Soc. Am. A* **35**, 1091–1102 (2018).

13 N. G. Worku and H. Gross, "Propagation of truncated gaussian beams and their application in modeling sharp-edge diffraction," *J. Opt. Soc. Am. A* **36**, 859–868 (2019).

14 A. W. Greynolds, "Ten years after (no, not the band): advancements in optical engineering computations over the decade(s)," in *Novel Optical Systems, Methods, and Applications XXIII*, C. F. Hahlweg and J. R. Mulley, Eds., 10, SPIE, (Online Only, United States) (2020).

15 J. W. Goodman, "Introduction to fourier optics," *Introduction to Fourier optics, 3rd ed., by JW Goodman. Englewood, CO: Roberts & Co. Publishers, 2005* **1** (2005).

16 Y. Cai and Q. Lin, "Decentered elliptical Gaussian beam," *Applied Optics Vol 41 No 21* , 5 (2002).

17 J. E. Harvey, R. G. Irvin, and R. N. Pfisterer, "Modeling physical optics phenomena by complex ray tracing," *Optical Engineering* **54**(3), 1 – 12 (2015).

18 J. N. Ashcraft and E. S. Douglas, "An open-source gaussian beamlet decomposition tool for modeling astronomical telescopes," *Modeling, Systems Engineering, and Project Management for Astronomy IX* (2020).

19 M. D. Perrin, R. Soummer, E. M. Elliott, *et al.*, "Simulating point spread functions for the James Webb Space Telescope with WebbPSF," in *Space Telescopes and Instrumentation 2012: Optical, Infrared, and Millimeter Wave*, M. C. Clampin, G. G. Fazio, H. A. MacEwen, *et al.*, Eds., **8442**, 1193 – 1203, International Society for Optics and Photonics, SPIE (2012).

20 T. M. Jeong, D.-K. Ko, and J. Lee, "Generalized ray-transfer matrix for an optical element having an arbitrary wavefront aberration," *Opt. Lett.* **30**, 3009–3011 (2005).

21 B. D. Stone and G. W. Forbes, "Differential ray tracing in inhomogeneous media," *J. Opt. Soc. Am. A* **14**, 2824–2836 (1997).

22 A. W. Greynolds, "Vector Formulation Of The Ray-Equivalent Method For General Gaussian Beam Propagation," in *Current Developments in Optical Engineering and Diffraction Phenomena*, R. E. Fischer, J. E. Harvey, and W. J. Smith, Eds., **0679**, 129 – 133, International Society for Optics and Photonics, SPIE (1986).

23 S. K. Lam, A. Pitrou, and S. Seibert, "Numba: A llvm-based python jit compiler," in *Proceedings of the Second Workshop on the LLVM Compiler Infrastructure in HPC*, 1–6 (2015).

## 5 Acknowledgments

This research made use of High Performance Computing (HPC) resources supported by the University of Arizona TRIF (Technology and Research Initiative Fund), UITS, and Research, Innovation, and Impact (RII) and maintained by the UArizona Research Technologies department. This work was funded by a NASA Space Technology Graduate Research Opportunity.

**Jaren N. Ashcraft** is a Ph.D. Candidate at the University of Arizona's Wyant College of Optical Sciences. He recieved his B.S. degree in Optical Engineering from the University of Rochester, and M.S. degree in Optical Sciences from the University of Arizona. He is a recipient of the NASA Space Technology Graduate Research Opportunity.

Biographies and photographs of the other authors are not available.

# List of Figures

# List of Tables